

# The Adaptive Buffered Force QM/MM method in the CP2K and AMBER software packages

Letif Mones <sup>\*</sup>, Andrew Jones <sup>†</sup>, Andreas W. Götz <sup>‡</sup>, Teodoro Laino <sup>§</sup>,  
Ross C. Walker <sup>‡,¶</sup>, Ben Leimkuhler <sup>||</sup>, Gábor Csányi <sup>\*</sup>, Noam Bernstein <sup>\*\*</sup>

February 17, 2022

## Abstract

The implementation and validation of the adaptive buffered force QM/MM method in two popular packages, CP2K and AMBER are presented. The implementations build on the existing QM/MM functionality in each code, extending it to allow for redefinition of the QM and MM regions during the simulation and reducing QM-MM interface errors by discarding forces near the boundary according to the buffered force-mixing approach. New adaptive thermostats, needed by force-mixing methods, are also implemented. Different variants of the method are benchmarked by simulating the structure of bulk water, water autoprotolysis in the presence of zinc and dimethyl-phosphate hydrolysis using various semiempirical Hamiltonians and density functional theory as the QM model. It is shown that with suitable parameters, based on force convergence tests, the adaptive buffered-force QM/MM scheme can provide an accurate approximation of the structure in the dynamical QM region matching the corresponding fully QM simulations, as well as reproducing the correct energetics in all cases. Adaptive unbuffered force-mixing and adaptive conventional QM/MM methods also provide reasonable results for some systems, but are more likely to suffer from instabilities and inaccuracies.

**Keywords:** QM/MM, adaptive QM/MM, force-mixing, multi scale ■

---

<sup>\*</sup>Engineering Department, University of Cambridge, Cambridge, CB2 1PZ, United Kingdom

<sup>†</sup>School of Physics and Astronomy, University of Edinburgh EH9 3JZ, United Kingdom

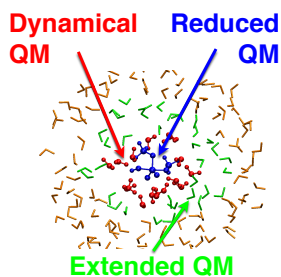
<sup>‡</sup>San Diego Supercomputer Center, University of California San Diego, La Jolla, California 92093, United States

<sup>§</sup>IBM Research–Zurich, Säumerstrasse 4, 8803 Rüschlikon, Switzerland

<sup>¶</sup>Department of Chemistry and Biochemistry, University of California San Diego, La Jolla, California 92093, United States

<sup>||</sup>The Maxwell Institute and School of Mathematics, University of Edinburgh EH9 3JZ, United Kingdom

<sup>\*\*</sup>Naval Research Laboratory, Center for Computational Materials Science, Washington, DC 20375, United States of America



We present implementations of an adaptive method for QM/MM simulations in the AMBER and CP2K packages which make it straightforward to describe quantum mechanically not only the reacting species, but also a surrounding region of solvent, because the set of quantum atoms can be changed at will during the simulation. We compare geometries and free energy profiles to those of fully quantum mechanical simulations and show that our scheme is more robust than alternatives.

# INTRODUCTION

Quantum-mechanics/molecular-mechanics (QM/MM) methods<sup>1</sup> have matured over the past few decades and are now an essential tool for modeling chemical reactions of complex systems. Most of the system is described by typically non-reactive MM force fields, but these give a poor (or even no) description of chemical processes such as changing charge state or covalent bond rearrangement. A quantum mechanical description is used in the region where such processes occur, and the extent of this region is kept small due to the associated computational expense. The QM and MM subsystems affect each other directly, by covalent, electrostatic, or other non-bonded interactions, as well as implicitly through long-range structure in the MM subsystem. Capturing such long range interactions can be essential even for the description of the local structure, e.g. a in protein where the reaction involves residues that are kept in place by the structure of the rest of the protein, or because long range electrostatic effects play a direct role in the reaction.<sup>2,3</sup>

For a QM/MM method to describe the complete system accurately, the individual methods used for the QM and MM descriptions must be appropriate for the configurations and processes in their respective regions, and the interaction between them must be accounted for. The dominant approach, which we will call *conventional* QM/MM (conv-QM/MM), is to fix the set of atoms in the QM and MM subsystems and define the total energy of the system as a sum of the QM energy of the QM region, the MM energy of the MM region, and an interaction energy. The interaction term can include the non-bonded and electrostatic energies of MM descriptions of the QM atoms in the field of the MM atoms (“mechanical embedding”),<sup>4</sup> or it may include the effect of the MM electrostatic field on the QM description, including the explicitly described electron density (“electrostatic embedding”).<sup>4</sup> If covalent bonds across the QM-MM interface are present, they must be capped in some way in the QM description so as to eliminate dangling bonds in the QM subsystem, e.g. using H atoms<sup>5</sup>, generalized hybrid orbitals<sup>6</sup> or pseudopotentials<sup>7</sup>. The accuracy of the conventional approach depends on the appropriateness of using a fixed set of atoms in the QM region, and on the ability of the QM-MM interaction term to eliminate the fictitious boundary effects in the QM and MM subsystem calculations.

Carrying out QM/MM simulations on different sized QM regions shows that widely used interaction terms lead to significant errors in the atomic forces near the QM-MM interface when compared to calculations using very large QM regions or describing the entire system quantum mechanically using periodic boundary conditions (we will refer to the latter as “fully QM”).<sup>8–11</sup> Although in many cases the effect on relevant observables can be small, these errors can be very problematic when the set of QM atoms is allowed to change. In such adaptive methods,<sup>12–19</sup> which are used to enable the QM region to move or species to diffuse in or out of the reaction site, errors near the interface can lead to an instability and a net flux of atoms between the QM and MM regions resulting in unphysical density variations.<sup>20,21</sup>

There are a number of fundamental issues that must be addressed in the design of any method that couples different descriptions in different regions of a single system. The way they are addressed can have particular implications for adaptive simulations, which may be different from the way the choices affect simulations where the set of atoms in each subsystem is fixed. One choice is whether the coupling is formulated in terms of energy<sup>13,15,16,18,19,22</sup> or forces<sup>12,14,17,20,21,23–25</sup>. If it is formulated in terms of energy, the total energy of the coupled system can be defined, and changes of that energy as atoms or molecules switch between descriptions can adversely affect the simulation. This can be represented as a difference in chemical potential of the switching species being described with the two models. A mismatch at any point in space for any molecular conformation will lead to unphysical forces on atoms as they switch description, leading to transport of atoms to the lower chemical potential region. Coupling in terms of forces can avoid this chemical potential mismatch effect, at the cost of forgoing energy conservation because no total energy can be defined, due to the non-conservative nature of the forces used to drive the dynamics. This tradeoff motivated the choice to use a force-based approach both in our work, the Hot Spot<sup>12</sup> and difference-based adaptive solvation (DAS)<sup>17</sup> methods. The use of non-conservative forces would lead to unstable molecular dynamics trajectories, which we avoid by using adaptive thermostats. These have been shown to sample the correct distribution even in the presence of net heat generation.<sup>26</sup>

Another choice is whether the transition between the two descriptions is abrupt or continuous. An abrupt transition leads to discontinuities in the dynamics as atoms suddenly

switch from one region to another. Employing a transition region can make the energy or forces continuous by smoothly interpolating between multiple calculations, but increases the number of force calculations that must be performed. While many published methods use transition regions to smooth out such switching discontinuities,<sup>12-19,27</sup> we have found that using abrupt transitions within a force-mixing approach does not seem to significantly affect the accuracy of average structures and free energy profiles.<sup>20,21,28</sup>

The third choice is how the errors near the interface between the two regions are handled. Energy based methods are formulated in terms of an MM energy, a QM energy, and the interaction term, and the accuracy of the last one determines this error. Adaptive methods like ONIOM-XS<sup>13</sup> and SAP<sup>15,16</sup> simply combine a weighted sum of several such calculations, and therefore include a weighted sum of interface related errors. Methods that mix a quantity that can be localized to each atom can, in general, improve on this using buffers, as we explain below. Because the energy, especially in the QM description, can not be localized to each atom, such mixing is generally applied to forces.<sup>12,14,17,19</sup> The buffer regions used to improve boundary force errors are conceptually distinct from the transition regions mentioned above that help smooth discontinuities.

Over the past few years we have developed the adaptive buffered-force QM/MM method (adbf-QM/MM), which uses force-mixing, abrupt transitions, and buffers to reduce the effect of interface errors and enable stable adaptive simulations.<sup>20</sup> Many other published methods can also be characterized in terms of the above choices. The ABRUPT method<sup>19</sup> is equivalent to a conv-QM/MM simulation, using energy based coupling, where atoms switch abruptly between the two descriptions without buffers. The Hot Spot method<sup>12</sup> uses force-mixing with transitions that are interpolated over a region of about 0.5 Å, but no buffers. Sorted adaptive partitioning (SAP)<sup>15</sup>, ONIOM-XS<sup>13</sup>, and difference-based adaptive solvation (DAS)<sup>17</sup> all use smooth transitions and no buffers, but the first two use an energy based coupling while the last uses force-mixing. The SAP and DAS methods require one calculation per molecule in the transition region, and the ONIOM-XS method is limited to a single molecule in that region.

In previous publications we tested the adbf-QM/MM method on the structure of bulk water,<sup>20</sup> as well as the free energy profiles of two reactions in water, nucleophilic substitution

in methyl chloride and the deprotonation of tyrosine.<sup>21</sup> Here we describe the implementation of the adbf-QM/MM method in two popular software packages, CP2K<sup>29</sup> and AMBER.<sup>30,31</sup> The implementation extends the QM/MM capabilities of the packages, and with appropriate choice of parameters can be used to carry out adaptive QM/MM simulation with or without buffering and force-mixing. We test the different variants using a variety of QM models, including density functional theory (DFT) and semi-empirical quantum mechanical (SE) models, on the structure of bulk water, the free energy profiles of dimethyl-phosphate hydrolysis and the autoprotolysis of water in the presence of a zinc ion.

## METHODOLOGY

### Overview of Adaptive Buffered Force QM/MM method

In the adbf-QM/MM method the atomic forces that are used in molecular dynamics simulations to generate a trajectory are obtained by combining two QM/MM force calculations. A flowchart describing the force calculations is shown in Fig. 1. At each time step, the system is partitioned into a number of different regions, which are defined as follows. We begin by creating two sets of atoms, the first consisting of atoms that should follow trajectories using QM forces (we call this the *dynamical QM region*), and those that should follow MM forces (*dynamical MM region*). The first and more expensive QM/MM calculation (“extended QM/MM calculation”) uses an enlarged QM region to obtain accurate forces for atoms in the dynamical QM region. This extended QM region is constructed by adding a *buffer region* around the dynamical QM region. The buffer region size required to reduce the force errors at the QM-MM boundary below a preset threshold can be determined from the convergence of forces in the dynamical QM region as a function of buffer region size, carried out separately before the production run on a few relevant configurations (e.g. near the estimated extrema of a free energy profile).

The second QM/MM calculation (“reduced QM/MM calculation”) uses a smaller QM region (which we call the *core region*) to reduce force errors due to the QM-MM boundary on atoms in the MM region. When the necessary force field parameters are available, the

core region may be eliminated altogether and this reduced size QM/MM calculation replaced by a cheap fully MM calculation. The forces for the propagation of the dynamics are then obtained based on the current identity of the atoms:

$$\mathbf{F}_i = \begin{cases} \mathbf{F}_i^{\text{Extended}}, & \text{if } i \in \text{dynamical QM region} \\ \mathbf{F}_i^{\text{Reduced}}, & \text{if } i \in \text{dynamical MM region} \end{cases} \quad (1)$$

This is a so-called abrupt force-mixing scheme, where forces used for dynamics switch from one description to the other without a transition region. When an atom is switched from the dynamical QM region to the dynamical MM region or vice versa, the force it experiences has a discontinuity. Introducing a narrow transition region in which the dynamical force is a linear combination of the forces calculated in the extended and reduced QM/MM calculations would smooth out this discontinuity.<sup>12,13,15,17</sup>

Adaptivity is achieved by defining criteria to select atoms for the various regions that are dynamically evaluated at each time step during the simulation. In our implementation each region is composed of a list of atoms fixed by the user due to their chemical role and additional atoms that are selected due to their distance from atoms in other regions. First, the core region is created by combining the fixed list and nearby atoms, based on a cutoff distance,  $r_{\text{core}}$ , from the atoms in the fixed list. Next, the dynamical QM region is defined as the union of the core region, another (optional) fixed list and atoms within a cutoff distance,  $r_{\text{qm}}$ , of core region atoms. Finally the buffer region is defined as the union of yet another optional fixed list and atoms within a cutoff distance,  $r_{\text{buffer}}$ , from atoms in the dynamical QM region. An example of these regions from a simulation of the hydrolysis of dimethyl phosphate (at the transition state) is shown in Fig. 2. To reduce the frequency of switching between regions for atoms that are close to the boundary, *hysteresis* is applied to all distance cutoffs, so an atom has to come closer than some inner radius to become incorporated into a region, but must move farther than a larger, outer radius to be removed from the region.

The use of force-mixing has two direct consequences stemming from the lack of a total potential energy for the system. First, because the forces are not the derivatives of any energy function, the dynamics are not conservative. Any deviation from linear momentum conservation is easily fixed exactly by adding a small correction force to some or all atoms, but the deviation from energy conservation necessitates the use of an appropriate thermostat

to maintain the correct kinetic temperature throughout the system. We have found that a simple adaptive Langevin thermostat<sup>26</sup> (described below) is sufficient to give a stable and spatially uniform temperature profile.<sup>21</sup> Second, the lack of a total energy prevents the use of some free energy calculation methods, although potential of mean force methods, which require only forces and trajectories, can still be applied.<sup>21</sup>

By appropriately setting the cutoff distances for the various regions, the adbf-QM/MM method can be made to be equivalent to a number of other adaptive methods which we compare to here. The adaptive conventional QM/MM method (adconv-QM/MM), which is an energy-mixing scheme and is equivalent to the ABRUPT method<sup>19</sup>, corresponds to setting the core and dynamical QM regions to be the same and an empty buffer region. The adaptive unbuffered force-mixing QM/MM method (adubf-QM/MM), which is very close to the hot spot method,<sup>12</sup> corresponds to an empty (or minimal) core region, an adaptive dynamical QM region, and an empty buffer region. The difference between the adconv-QM/MM and adubf-QM/MM methods lies therefore in how the dynamical forces for the MM atoms are obtained. In the adconv-QM/MM method there is only one QM/MM force calculation, and the MM atoms are propagated using the forces from this same QM/MM force calculation that yields the forces for the QM atoms. In the adubf-QM/MM method, which is a true force-mixing approach, the MM atoms are propagated with forces obtained from either a fully MM calculation or a reduced QM/MM calculation with a very small QM region which includes just the reactants. In addition, we also compare our results to a conv-QM/MM simulation, which is not adaptive, so only the solutes are treated quantum mechanically.

## **Implementations of Adaptive Buffered Force QM/MM method**

We have implemented adbf-QM/MM in two popular QM/MM programs: the AMBER package<sup>30</sup>, which has a number of built in SE methods as well as an interface to external QM programs, and CP2K, which is primarily a DFT package but contains some SE models<sup>29</sup>. Because of the different structure of the two codes, the actual implementations are slightly different, so we begin here with the common and general concepts needed to specify an adbf-QM/MM calculation. In addition to the general QM/MM keywords used by each program the user has to specify only a few additional variables. The most important ones control the



inclusion of atoms in the various regions:

- Specification of a disjoint list of fixed core, dynamical QM and buffer atoms. In CP2K the fixed core region cannot be empty; otherwise these lists are optional.
- Specification of the hysteretic inner ( $r_{\text{in}}$ ) and outer ( $r_{\text{out}}$ ) radii of the adaptive core, dynamical QM and buffer regions.

Both the CP2K and AMBER implementations take special care with covalent bonds crossing the interfaces in the reduced and extended QM/MM calculations. To minimize errors associated with breaking such covalent bonds indiscriminately, only entire molecules or fragments bounded by particular covalent bonds are included or excluded from each region. In CP2K the specific covalent bonds that can be cut by the reduced and extended calculations' interfaces must be fixed in the input file, and large molecules (such as proteins) that should not be entirely included or excluded must therefore be omitted from the adaptive region selection. The AMBER implementation supports an adaptive definition of breakable covalent bonds at the interfaces.

Both implementations support different ways of applying the momentum conservation correction. The CP2K implementation supports different total charges of the QM region in the reduced and extended calculations, as well as constructing the dynamical QM region based only on distances from the fixed subset of the core region. The AMBER implementation automatically adjusts the total charge in the reduced and extended QM/MM calculations based on a default table of oxidation numbers of the adaptively selected atoms. This table can be modified by the user, and the AMBER implementation also supports a number of different geometrical criteria for adaptive core, dynamical QM, and buffer selection.

Adaptive thermostats required for adbf-QM/MM dynamics have been implemented, including support for independent thermostats for each degree of freedom, using the adaptive Langevin<sup>26</sup> method (CP2K and AMBER) and several variants of the adaptive Nosé-Hoover<sup>26,32,33</sup> method (AMBER only). The adaptive Langevin thermostat is essentially a Langevin thermostat (to ensure ergodicity) in parallel with a Nosé-Hoover thermostat (to compensate for deviations from energy conservation), and the corresponding dynamical

equations are

$$\dot{q} = \frac{p}{m} \quad (2)$$

$$\dot{p} = F(q) - (\gamma + \chi)p + \sqrt{2k_B T \gamma m} \dot{w} \quad (3)$$

$$\dot{\chi} = (2K - nk_B T) / Q. \quad (4)$$

The position and momentum vectors are  $q$  and  $p$ , respectively,  $\chi$  is the Nosé-Hoover degree of freedom,  $m$  is the atomic mass, and  $F(q)$  is the force. The temperature is  $T$ , Boltzmann's constant is  $k_B$ ,  $K$  is the kinetic energy, and  $n$  is the number of degrees of freedom associated with the thermostat. The Langevin friction is  $\gamma = 1/\tau_L$  where  $\tau_L$  is the Langevin time constant, the Nosé-Hoover fictitious mass is  $Q = k_B T \tau_{\text{NH}}^2$  where  $\tau_{\text{NH}}$  is the Nosé-Hoover time constant, and  $\dot{w}$  is the time derivative of a Wiener process. The adaptive Nosé-Hoover method has a similar structure, but the Langevin thermostat is replaced with Nosé-Hoover chains with an optional Langevin thermalization of the last thermostat in the chain. In its most general form this gives the adaptive Nosé-Hoover-chains-Langevin method with the corresponding equations

$$\dot{q} = \frac{p}{m} \quad (5)$$

$$\dot{p} = F(q) - (\xi_1 + \chi)p \quad (6)$$

$$\dot{\xi}_1 = (2K - nk_B T) / Q_1 - \xi_1 \xi_2 \quad (7)$$

$$\dot{\xi}_2 = (Q_1 \xi_1^2 - k_B T) / Q_2 - \xi_2 \xi_3 \quad (8)$$

...

$$\dot{\xi}_r = (Q_{r-1} \xi_{r-1}^2 - k_B T) / Q_r + \sqrt{2k_B T \gamma_l Q_r} \dot{w} - \gamma_l \xi_r \quad (9)$$

$$\dot{\chi} = (2K - nk_B T) / Q, \quad (10)$$

where  $r$  is the length of the chain,  $\xi_i$  and  $Q_i$  are the Nosé-Hoover chain degrees of freedom and their masses, respectively, and  $\gamma_l$  is the Langevin friction for thermalizing the final thermostat in the chain. Setting  $r$  to 1 corresponds to the adaptive Nosé-Hoover-Langevin thermostat, while omitting the Langevin part (i.e. formally setting  $\gamma_l$  to 0) with  $r > 1$  results in the adaptive Nosé-Hoover-chain.

Both adaptive thermostats can be applied so that a separate NH variable (or NH chain) is coupled to each degree of freedom<sup>34</sup>, rather than a single NH variable coupling to the

total kinetic energy. This is the mode in which we use adaptive thermostats in this work, because in the nonconservative force-mixing simulations extra heat is generated locally near the QM-MM interface and the amount that needs to be dissipated therefore varies in space.

The sections of example CP2K and AMBER input files that are relevant to the adbf-QM/MM implementations are shown in Fig. 3. The CP2K inputs consist of a `&QMMM` section to specify the fixed core list, a `&FORCE_MIXING` section to specify the other regions and momentum conservation details, and a `&THERMOSTAT` section with a `REGION MASSIVE` keyword and an `&AD_LANGEVIN` section specifying the two time constants. The AMBER input specifies the thermostat with the `ntt` keyword (6, 7 and 8 for the adaptive Langevin, adaptive Nosé-Hoover chains and adaptive Nosé-Hoover chains with Langevin, respectively), activates the QM/MM functionality, and enables force-mixing in the `&qmmm` section with the `abfqmmm=1` keyword. In this section the input file also sets the momentum conservation details, fixed lists and adaptive core, dynamical QM, and buffer radii, as well as the charges of the three regions. Example input files are included as supplementary information, however these do not show every available option, and full details are available in the documentations of the two packages.

## Model Systems

To test the adaptive QM/MM implementations we studied structure and reaction free energy profiles in three systems. In pure bulk water, which provides a stringent test for adaptive methods as previous work has shown,<sup>20</sup> we studied the structure for a number of QM models and adaptive QM/MM methods. For two reactions in water solution, the autoprotolysis of water in the presence of a  $\text{Zn}^{2+}$  ion and the hydrolysis of dimethyl-phosphate, we calculated the free energy profile using a number of adaptive QM/MM methods. In all cases we compared to reference calculations employing a fully QM description using smaller simulation cells, and for the autoprotolysis of water we also ran fully QM simulations using an intermediate size unit cell. The QM region sizes for all QM/MM simulations are summarized in Table 1. Adaptive radii were applied to distances between all atoms, except for SE bulk water simulations where only O-O distances were used to select molecules. The sum of core and dynamical QM radii were chosen to ensure that the first hydration shell is included in

Simulation type	$r_{\text{core}}$ (Å)	$r_{\text{qm}}$ (Å)	$r_{\text{buffer}}$ (Å)
<i>SE Bulk water</i>			
adbf-QM/MM	0.0 – 0.0	4.0 – 4.5 (*)	4.0 – 4.5 (*)
<i>MNDOd Autoprotolysis reaction</i>			
conv-QM/MM	0.0 – 0.0	0.0 – 0.0	0.0 – 0.0
adconv-QM/MM	2.5 – 3.0	0.0 – 0.0	0.0 – 0.0
adubf-QM/MM	0.0 – 0.0	2.5 – 3.0	0.0 – 0.0
adbf-QM/MM	0.0 – 0.0	2.5 – 3.0	3.0 – 3.5
<i>DFT bulk water and dimethyl-phosphate hydrolysis</i>			
conv-QM/MM	0.0 – 0.0	0.0 – 0.0	0.0 – 0.0
adconv-QM/MM	3.0 – 3.5	0.0 – 0.0	0.0 – 0.0
adubf-QM/MM	0.0 – 0.0	3.0 – 3.5	0.0 – 0.0
adbf-QM/MM	0.0 – 0.0	3.0 – 3.5	3.0 – 3.5

Table 1: Adaptive region radii for the QM/MM simulations, applied to all interatomic distances, except for SE bulk water simulations (\*), where the selection criterion was based only on the oxygen–oxygen distances.

the dynamical QM region.

All systems were simulated using constant temperature and volume molecular dynamics. For bulk water the structure was analyzed by calculating the time averaged radial distribution function (RDF) for a molecule at the center of the dynamical QM region. Free energy profiles were calculated using umbrella integration (UI)<sup>35</sup>, with a bias potential

$$V_{\text{restraint}} = \frac{1}{2}k (x(\mathbf{r}) - x_0)^2$$

where  $k$  is the curvature,  $x_0$  is the desired value of the collective coordinate, and  $x(\mathbf{r})$  is its instantaneous value. In the biased simulation the mean gradient of the bias potential is approximately equal to the negative of the gradient of the potential of mean force (PMF) at the mean value of the collective coordinate<sup>35</sup>. For simulations with AMBER the bias was achieved using the PMFlib package<sup>36</sup> that was linked to AMBER, and for CP2K internal

subroutines were used.

### *Bulk water structure*

For bulk water we used cubic simulation cells with 13.8 Å (93 molecules) and 41.9 Å (2539 molecules) sides for the fully QM and QM/MM calculations, respectively. The MM water molecules were described with the flexible TIP3P (fTIP3P) potential.<sup>37</sup> We used the AMBER implementation to compare the results of the adbf-QM/MM method for a number of SE models. In each simulation a single water molecule was selected to be the center of the dynamical QM region, with radii listed in Table 1 applied only to O-O distances when selecting molecules for the adaptive regions. No core region was used, so the reduced size calculation was done as a fully MM calculation. The SE models compared were MNDO<sup>38</sup>, AM1<sup>39</sup>, AM1d<sup>40</sup>, AM1disp<sup>41</sup>, PM3<sup>42</sup>, PM3-MAIS<sup>43</sup>, PM6<sup>44</sup>, RM1,<sup>45</sup> and DFTB<sup>46</sup>. Using the CP2K implementation we compared the results of various QM/MM methods<sup>47,48</sup> with DFT and the BLYP exchange-correlation functional<sup>49–51</sup> plus Grimme’s van der Waals correction,<sup>52,53</sup> with a DZVP basis, GTH pseudopotentials,<sup>54</sup> and a density cutoff of 280 Ry. The methods compared were conv-QM/MM, adubf-QM/MM, adconv-QM/MM, and adbf-QM/MM. In this case a single water molecule was selected for the fixed core region, with adaptive radii listed in Table 1 applied to all interatomic distances.

### *Reaction free energy profiles*

Water related proton transfer reactions can be facilitated by the presence of divalent metal ions<sup>55</sup>. The metal ion lowers the  $pK_a$  of the coordinated water molecule making it a stronger acid. Our example is a very simple model of this phenomenon, the proton transfer reaction between a zinc-coordinated water molecule (proton donor) and a non-coordinated water molecule (proton acceptor) in water solution, shown in Fig. 4. To calculate the free energy profile for this reaction we used UI with the collective coordinate being the difference between rational coordination numbers ( $DRCN$ ) of the acceptor and donor oxygen atoms<sup>56,57</sup>:

$$DRCN(\{\mathbf{r}_{HO_D}, \mathbf{r}_{HO_A}\}) = RCN(\{\mathbf{r}_{HO_A}\}) - RCN(\{\mathbf{r}_{HO_D}\}) \quad (11)$$

and

$$RCN\left(\left\{\mathbf{r}_{HO_{D/A}}\right\}\right) = \sum_i^{\text{H atoms}} \frac{1 - \left(\frac{r_i}{r_0}\right)^\alpha}{1 - \left(\frac{r_i}{r_0}\right)^\beta}, \quad (12)$$

where the subscripts  $D$  and  $A$  denote the donor and acceptor oxygen atoms, respectively,  $\alpha = 6$ ,  $\beta = 18$  and the reference distance  $r_0 = 1.6 \text{ \AA}$ .

The reactions were simulated in cubic cells with sides of  $13.6 \text{ \AA}$  (87 water molecules) and  $17.2 \text{ \AA}$  (174 water molecules) for the fully QM and  $45.8 \text{ \AA}$  (3303 water molecules) for the QM/MM simulations. The simulations were carried out using the AMBER implementation with  $\text{Zn}^{2+}$  ion parameters from Ref.<sup>58</sup>, fTIP3P model for MM waters,<sup>37</sup> and the MNDO(d) SE method.<sup>59</sup> The  $\text{Zn}^{2+}$  ion and two reactant water molecules were defined as the QM region in the conv-QM/MM simulation, as well as the fixed core region in the adaptive simulations. Adaptive regions used radii listed in Table 1 with all interatomic distances and only entire water molecules included or excluded in any region.

In all autoprotolysis simulations we applied one-sided harmonic restraints for the following 3 distances: one between the two O atoms beyond  $3.0 \text{ \AA}$  to keep the reactants together, another between the O atom of donor water molecule and zinc ion beyond  $2.5 \text{ \AA}$  to keep the donor water molecule in the coordination sphere of the metal ion, and the third between the O atom of acceptor water molecule and zinc ion for distances larger than  $3.5 \text{ \AA}$  to prevent the acceptor water molecule from entering into the coordination sphere of the metal ion. For each restraint a force constant of  $25.0 \text{ kcal mol}^{-1} \text{ \AA}^{-2}$  was applied. The applied force constant for the UI restraint was  $400 \text{ kcal mol}^{-1}$  and the profile was calculated in the range of  $DRCN \in [-0.2, 2.2]$ .

The second reaction we simulated was dimethyl-phosphate hydrolysis, shown in Fig. 5, where an incoming hydroxide ion attacks the dimethyl-phosphate and causes a methoxide ion to leave. A similar hydrolysis of phosphate diesters in solution is a biologically important type of phosphoryl transfer reactions and a key model to understand DNA cleavage<sup>60</sup>. The reaction coordinate for the UI procedure was the distance difference between the leaving O-P atoms and the attacking O-P atoms

$$DD(\mathbf{r}_{\text{PO}_L}, \mathbf{r}_{\text{PO}_A}) = |\mathbf{r}_{\text{PO}_L}| - |\mathbf{r}_{\text{PO}_A}|, \quad (13)$$

where  $L$  and  $A$  designate the leaving and attacking O atoms, respectively. The reaction was simulated in cubic cells with sides of  $13.6 \text{ \AA}$  (86 water molecules) and  $48.4 \text{ \AA}$  (3903 water molecules) for the fully QM and QM/MM simulations, respectively.

Because our simulation protocol starts with an MM relaxation, MM parameters were needed for the solutes. The charges of the phosphate and hydroxide were calculated according to the standard procedure<sup>61,62</sup>, while the bonded and vdW parameters of the phosphate were derived from the ff99SB version of the AMBER force field<sup>63</sup>, and the water molecules were described by the fTIP3P model.<sup>37</sup> For the hydroxide ion the same parameters were used as for the fTIP3P. For the DFT model the BLYP exchange-correlation functional<sup>49–51</sup> was applied with Grimme’s van der Waals correction,<sup>52,53</sup> using the DZVP basis set with GTH pseudopotentials<sup>54</sup> and a density cutoff of 280 Ry. The QM region of the conv-QM/MM calculation and the fixed core region of the adaptive QM/MM calculations consisted only of the reactant dimethyl-phosphate and hydroxide. Adaptive regions used the radii listed in Table 1 with all interatomic distances and only entire water molecules selected for inclusion or exclusion. The free energy profile was carried out in the range of  $DD \in [-3.0, 3.0]$  Å using an UI restraint force constant of 400 kcal mol<sup>-1</sup> Å<sup>-1</sup>.

## Simulation protocol

### *General simulation parameters*

All simulations used periodic boundary conditions with MM-MM electrostatic interactions calculated by the Ewald<sup>64</sup> and particle-mesh Ewald<sup>65</sup> for the small and large simulation cells, respectively. For fully SE and DFT simulations, the CP2K package was used with the smooth particle mesh Ewald method and multipole expansion up to quadrupoles.<sup>66</sup> In the AMBER QM/MM simulations the QM-MM interactions were calculated using a multipole description within 9 Å while both the long-range QM-QM and QM-MM electrostatic interactions were based on the Mulliken charges of the QM atoms according to Ref.<sup>67–70</sup>. In the CP2K QM/MM simulations the QM-MM interaction used Gaussian smearing of the MM charges.<sup>47</sup> When systems were charged a uniform background countercharge was applied. Molecular dynamics simulations with a time step of 0.5 fs were used for equilibration and canonical ensemble sampling.

The first step in the simulation protocol was to generate independent initial configurations for all box sizes from long equilibrium fully MM simulations. In the case of bulk water all fully QM and QM/MM simulations were started from these MM equilibrated configurations.

For the reactions, first the relatively computationally inexpensive conv-QM/MM simulations were carried out starting from an initial configuration that was taken from a fully MM equilibrium simulation at the initial restraint position corresponding to the reactant state. The restraint forces for UI were sampled for some time period, and the restraint center was slowly changed to the next collective coordinate value, then the process repeated until the desired range of values were sampled. The more computationally expensive fully QM and adaptive QM/MM simulations were started from the final configuration of each conv-QM/MM trajectory at each restraint center position.

#### *Initial configurations*

The systems and topologies for investigating the bulk water were created by the Leap program of the AMBER package<sup>30</sup>. The initial geometries were relaxed for 5000 minimization steps, followed by a molecular dynamics *NVT* simulation of heating from  $T = 0$  K to  $T = 300$  K over 50 ps followed by 50 ps at fixed temperature. The density was then relaxed by a 200 ps *NpT* simulation at  $T = 300$  K and  $p = 1$  bar, and then the average box size was calculated during an additional 500 ps long *NpT* simulation. During this last stage 10 independent configurations were selected at 50 ps intervals, which were all rescaled to the mean volume. Finally, for each of the 10 configurations a 500 ps long *NVT* simulation was carried out at 300 K. In each case the temperature was controlled by a Langevin thermostat<sup>71</sup> with a friction coefficient of  $5 \text{ ps}^{-1}$ . The systems for the reactions were also generated using the Leap program of the AMBER package<sup>30</sup> to surround the reactants by water molecules. These starting configurations were equilibrated by the same procedure as for the bulk water systems.

#### *Water autoprotolysis*

Conventional QM/MM simulations were carried out using AMBER and PMFlib for *DRCN* from -0.2 to 2.2 in increments of 0.1. The restraint reaction coordinate was changed from its actual value in the reactant state to the starting value of -0.2 over 20 ps. Then, the *DRCN* was sequentially changed by 0.1 over 1 ps long trajectories, followed by simulation at fixed restraint position. Restraint force values for UI were collected for the number of initial configurations and trajectory lengths listed in Table 2. All simulations used a Langevin thermostat<sup>71</sup> with a friction coefficient of  $5 \text{ ps}^{-1}$ .



Simulation type	# of independent	Trajectory length per config.	
	configurations	total (ps)	used for analysis (ps)
<i>Bulk water</i>			
SE fully QM	10	10	5
SE adbf-QM/MM	10	50	40
DFT fully QM	5	10	9
<i>Autoprotolysis reaction</i>			
MNDOd fully QM	10	12	10
MNDOd conv-QM/MM	10	10	8
MNDOd adconv-QM/MM	10	5.5	4.5
MNDOd adubf-QM/MM	10	5.5	4.5
MNDOd adbf-QM/MM	10	5.5	4.5
<i>Dimethyl-phosphate hydrolysis reaction</i>			
DFT fully QM	5	5	2.5

Table 2: Configuration numbers and trajectory lengths

Fully QM simulations for both box sizes were carried out using CP2K, starting from relaxed conv-QM/MM configurations at each reaction coordinate value, with a number of independent initial configurations and trajectory lengths listed in Table 2. Temperature was controlled by the CSVr thermostat<sup>72</sup> with a time constant of 200 fs. Adaptive QM/MM simulations were carried out starting from relaxed conv-QM/MM for the number of initial configurations and trajectory lengths listed in Table 2. Because of the energy conservation violation of all the adaptive methods, temperature was controlled by adaptive Langevin thermostats<sup>26</sup>, one per degree of freedom, with a Langevin time constant of 200 fs and a Nosé-Hoover time constant of 200 fs.

*Dimethyl-phosphate hydrolysis*

Initial conditions for the DFT simulations were generated by a conv-QM/MM simulation with the AM1 SE method using the AMBER code for  $DD$  from  $-3.0 \text{ \AA}$  to  $3.0 \text{ \AA}$ . The  $DD$  was changed from its initial value to  $-2.0 \text{ \AA}$  over 20 ps. The  $DD$  was then changed by increments of  $0.1 \text{ \AA}$  over 1 ps, followed by equilibration for 10 ps at each  $DD$  value. All subsequent simulations were carried out using CP2K using one adaptive Langevin thermostat per degree of freedom with a Langevin time constant of 300 fs and a Nosé-Hoover time constant of 74 fs. Simulations with fully QM, conv-QM/MM, adconv-QM/MM, adubf-QM/MM, and adbf-QM/MM were carried out with the number of configurations and trajectory lengths listed in Table 2. Values of  $DD$  from  $-3.0 \text{ \AA}$  in increments of  $0.6 \text{ \AA}$ , with additional samples at  $DD = \pm 0.3 \text{ \AA}$  and  $DD = \pm 0.1 \text{ \AA}$ , were used to calculate the UI free energy profile.

## RESULTS

### Bulk water

We performed a force convergence test to determine the appropriate buffer radii by calculating the forces on an O atom in the center of the QM region of a conventional QM/MM calculation, as a function of QM region radius, using a number of SE methods. Here the radius of the QM region models  $r_{\text{buffer}}$  in the adbf-QM/MM method’s extended QM calculation, since it controls the distance between the molecule whose forces we are testing and the

QM-MM interface. The atomic configurations were taken from the 10 MM equilibrated configurations described in the Simulation Protocol subsection and the calculations were carried out with MNDO, AM1, PM3, PM6, RM1, and DFTB. The resulting force errors calculated with respect to reference forces from a 10 Å radius conventional QM/MM calculation are plotted in Fig. 6. For each QM method a similar behaviour is seen in the force convergence: the average force error goes below 2 kcal mol<sup>-1</sup> Å<sup>-1</sup> (and the maximum goes below 4 kcal mol<sup>-1</sup> Å<sup>-1</sup>) around  $r_{\text{buffer}} = 4.0$  Å, which was chosen as the lower limit of the buffer size for the dynamics. A similar behaviour was observed in the case of DFT (BLYP).<sup>20</sup> We also investigated forces on the hydrogen atoms (data not shown) and found a slightly faster convergence.

The oxygen–oxygen RDF averaged over 10 independent trajectories are plotted in Fig. 7. In the case of PM3 the fluid density gradually goes down in the dynamical QM region during the dynamics and longer simulations showed that this process is irreversible, leading to an almost complete depletion of water in the dynamical QM region. This phenomenon was previously observed in Ref.<sup>73</sup> and the significantly different diffusion behaviours of the QM and MM water molecules were suggested as a possible reason. The PM3-MAIS method, which is an extension to PM3 parametrised to accurately reproduce the intermolecular interaction potential of water, does not suffer from this problem. In contrast to PM3, for MNDO the water structure in the QM region is stable for the duration of our simulations but the RDF slightly differs from the fully QM result. As expected, using a larger QM region improves the structure in this case. We also note that the force convergence for the MNDO is the slowest among the examined potentials (Fig. 6), so a larger buffer region may further improve the RDF. In the case of PM6 and RM1, the adbf-QM/MM RDFs show a somewhat lower first peak compared to the fully QM structure. However, the RDFs remain stable for longer simulation times. Based on our data we are not able to exclude unambiguously the possibility that, similarly to PM3, a net flux of atoms leaving the dynamical QM region causes this discrepancy. Even if this is the case, the diffusion is much slower than for PM3. For DFTB and AM1 the adbf-QM/MM and fully QM RDFs match almost perfectly. We investigated two additional AM1 variants (AM1d and AM1disp) and found similar RDFs to the fully QM AM1 result. In general we see that the first peak is higher for the fully QM simula-

tions than those of adbf-QM/MM. Although using larger dynamical QM and buffer regions could potentially improve the agreement, the improvement may be limited by differences in how the long range interactions are calculated<sup>67,69,74</sup> in the fully QM and the adbf-QM/MM simulations due to limitations in the packages used (CP2K and AMBER, respectively).

In Fig. 8 we compare the O-O RDFs for DFT calculations using fully QM, conv-QM/MM, adconv-QM/MM, adubf-QM/MM, and adbf-QM/MM. All but adubf-QM/MM have a first neighbour peak at approximately the correct distance, but their heights vary greatly. In the conv-QM/MM calculation, where only a single water molecule is in the QM region, the first neighbour peak height is approximately double the fully QM value, indicating that inaccurate forces at the QM-MM interface are greatly distorting the structure around the QM water. In the adconv-QM/MM calculation, where the size of the dynamical QM region is increased using hysteretic radii of 3.0-3.5 Å, the peak height is greatly improved, but there is an excess of molecules just inside the QM-MM interface, leading to an unphysical second broad peak in the RDF centered around about 3.8 Å. In contrast, using force mixing without buffers in the adubf-QM/MM calculation leads to an emptying of the dynamical QM region, nearly completely eliminating the first neighbour peak. The adbf-QM/MM method comes closest to reproducing the fully QM structure. The first neighbour peak has the correct position and height, although the minimum near 3.2 Å has been replaced by a shoulder. This artifact may be caused by the nearby QM-MM interface, and could perhaps be corrected by a larger dynamical QM region. Note that the effect is already much less significant than the artifacts in the other adaptive methods. The cumulative RDFs in the bottom panel of Fig. 8 show corresponding differences between the methods. The conv-QM/MM curve shows a large bulge near the first peak, but then follows the fully QM curve at longer distances due to an overly deep minimum in the RDF that compensates for the excess first neighbours. The two unbuffered adaptive methods show significant deviations from fully QM, up for adconv-QM/MM which has an excess second RDF peak, and down for adubf-QM/MM which is missing the first peak. Our adbf-QM/MM results show better agreement with fully QM throughout the distance range, with a small offset to larger values starting after the first RDF peak due to the shoulder in the peak.

## Water autoprotolysis in the presence of a zinc ion

In the simulation of water autoprotolysis in the presence of a  $\text{Zn}^{2+}$  ion with the conv-QM/MM method, the QM region consists of the metal ion and the reactant water molecules. No additional water molecules from the zinc’s coordination sphere are included because they are mobile, i.e. can exchange with bulk phase water on the simulation time scale, and the conv-QM/MM method is not adaptive. A possible way to keep these waters in the dynamical QM region is to restrain them near the zinc ion<sup>75</sup>, or restrain the remaining waters away from the dynamical QM region<sup>76</sup>. However, such restraints can significantly affect the entropic part of the free energy<sup>57</sup> preventing the correct comparison of the free energy profiles of the different methods.

For the adaptive QM/MM simulations we found that  $r_{\text{qm}} = 2.5 - 3.0 \text{ \AA}$  was sufficient to include the first hydration shell around the zinc ion and the reactants. To obtain the values of  $r_{\text{buffer}}$  we carried out force convergence tests at geometries taken from the free energy profile extremum states (reactant, transition and product) from the conv-QM/MM simulation. The average and maximum force errors of the zinc, the donor and acceptor oxygen atoms (which together comprise the core region) and the oxygen atoms of non-reacting water molecules in the dynamical QM region are plotted in Fig. 9. We see that including the first hydration shell around the reactant water molecules is sufficient to reduce the force error on all atoms to below approximately  $2.5 \text{ kcal mol}^{-1} \text{ \AA}^{-1}$ , which we take to be an acceptable value. Similarly to bulk water, the hydrogen atoms have a slightly faster convergence (data not shown). Interestingly, force errors on the metal ion require  $r_{\text{buffer}} \geq 3.0 \text{ \AA}$  to reach equally small values, despite the fact that it is surrounded by QM waters in its first coordination sphere even without the use of a buffer region. The reason for this slow convergence is probably due to the metal ion’s high charge and polarizability, which cannot be fully screened by the coordinated water molecules. Based on the convergence of the force on metal ion and the non-reactive water molecules in the dynamical QM region we chose  $r_{\text{buffer}} = 3.0 - 3.5 \text{ \AA}$ . Since the force convergence test showed small errors on the reactants’ atoms (although not on the metal ion, which functions as a catalyst, not a reactant) even in the absence of any buffer region, it may be reasonable to carry out the simulations without a buffer.

We therefore also performed adconv-QM/MM and adubf-QM/MM simulations using our AMBER implementation.

The free energy profiles of the different adaptive QM/MM methods calculated with the CP2K and AMBER implementations are presented in Fig. 10. Since the formulations of the QM-MM interaction differ for the two programs, we show the corresponding profiles in different figures. For all cases  $DRCN = 0.0$  corresponds to the reactant state. We used the profile of the smaller fully QM unit cell size as reference, but as the larger fully QM unit cell size profile differs by less than  $0.025 \text{ kcal mol}^{-1}$  RMS, we conclude that the small QM unit cell profile is converged with respect to the unit cell size. The curve of the fully QM simulation indicates the transition state (TS) at around  $DRCN = 1.6$  with an activation barrier of  $48.5 \text{ kcal mol}^{-1}$  and a shallow minimum of the product state at  $DRCN \sim 1.8$  with a reaction free energy of  $47.8 \text{ kcal mol}^{-1}$ .

As the reaction proceeds the conv-QM/MM profile diverges from the rest. However, the deviation is much larger for the AMBER implementation than for CP2K. This is probably due to the differences in calculating the QM-MM interaction in the two programs; for example, the replacement of the point charges used in AMBER by Gaussians in CP2K may be reducing the overpolarization of the QM calculation by the MM region and leading to an improvement of the conv-QM/MM calculation. In contrast to conv-QM/MM, all of the adaptive methods accurately reproduce the fully QM results. The adconv-QM/MM and adubf-QM/MM profiles differ only slightly from the adbf-QM/MM one, in accord with the observation of the force convergence test, where a QM region that included the first hydration shell was sufficient to get force convergence on the atoms of the reactants, even without the use of a buffer region.

## Dimethyl-phosphate hydrolysis

To determine the sizes of the qm and buffer regions we carried out force convergence tests of the three key atoms of the system that are involved in the reaction coordinate  $DD$ : the phosphorus atom and the attacking and leaving oxygen atoms. First, we examined the effect of different buffer region sizes directly around the phosphate and hydroxide ions by varying  $r_{\text{buffer}}$  with  $r_{\text{qm}} = 0.0 \text{ \AA}$  (Fig. 11). In general we found a much slower force convergence

as compared to the water autoprotolysis, which can be explained by the highly negatively charged species in this system. For the oxygen atoms a similar behaviour of the profiles can be seen for all three  $DD$  values we investigated: without a buffer (i.e.  $r_{\text{buffer}} = 1.0 \text{ \AA}$ , which is too small to include any neighboring molecules) the error is about  $15\text{-}20 \text{ kcal mol}^{-1} \text{ \AA}^{-1}$ , and it goes down to  $5\text{-}6 \text{ kcal mol}^{-1} \text{ \AA}^{-1}$  using a buffer size of  $3.0\text{-}3.5 \text{ \AA}$ . This buffer size corresponds to the first hydration shell around the reactants, and applying a larger buffer size does not improve the force convergence. For the phosphorus atom the force convergence profile shows a similar behaviour but converges to a larger average force error of  $\sim 15 \text{ kcal mol}^{-1} \text{ \AA}^{-1}$ . Based on Fig. 11 we set  $r_{\text{qm}} = 3.0 - 3.5 \text{ \AA}$ . We also investigated the convergence of forces as a function of buffer region around a finite dynamical QM region ( $r_{\text{qm}} = 3.0 - 3.5 \text{ \AA}$ ). In this case we did not find any additional improvement of the force convergence, which is in agreement with the tail of the profiles in Fig. 11 and suggests that applying a buffer region beyond the dynamical QM region that includes the first hydration shell will not alter the free energy profile significantly. We tested this by using  $r_{\text{buffer}} = 3.0 - 3.5 \text{ \AA}$ , as in the other simulated systems, in the adbf-QM/MM calculations.

The free energy curves of the conventional and adaptive QM/MM simulations of the systems are shown in Fig. 12. All profiles are shifted to  $F = 0 \text{ kcal mol}^{-1}$  at  $DD = -3.0 \text{ \AA}$ . The fully QM profile has a maximum at  $DD = -0.3 \text{ \AA}$  with  $\Delta F^\ddagger = 22.0 \text{ kcal mol}^{-1}$ , indicating the transition state of the reaction. Within the range of the UI calculations ( $[-3.0, 3.0] \text{ \AA}$ ) the fully QM profile does not have minima as expected due to the repulsion of the negatively charged reactants and products. The conv-QM/MM simulations result in a wide flat region in the range  $[-0.6, 0.6] \text{ \AA}$  with a minimum at  $DD = 0.0 \text{ \AA}$ , indicating a possible intermediate metastable state rather than a transition state, although the observed minimum is shallower than the error bars. The top of the conv-QM/MM profile is lower by  $\sim 5 \text{ kcal mol}^{-1}$  than the peak of the fully QM curve, corresponding to an error of  $\sim 25\%$ . The adubf-QM/MM profile has a single well defined transition state, but its height is significantly overestimated compared to fully QM ( $\Delta F^\ddagger = 32.8 \text{ kcal mol}^{-1}$ ). In contrast to conv-QM/MM and adubf-QM/MM, both the adconv-QM/MM and adbf-QM/MM profiles are in good agreement with the fully QM profile.

To further investigate the source of these differences, we computed the RDFs between

the central phosphorous and all water oxygen atoms. Instead of using the RDF, which is noisy due to the relatively short simulation times, we calculated its integral (IRDF), shown in Fig. 13. For smaller distances (2.5-3.0 Å) the conv-QM/MM IRDF shows a higher water density around the reactants compared to the fully QM simulations. This is due to the ability of the MM hydrogen atoms to approach the pentavalent transition state too closely, leading to an overstabilization of the doubly negatively charged phosphate and resulting in a lower barrier. In the case of adubf-QM/MM the IRDF profile shows that an instability has pushed water molecules out of the dynamical QM region, decreasing the density for  $r$  at least up to 7 Å. This unphysically low density in the reaction region reduces the stabilization of the transition state by the nearby waters, in accord with the higher barrier observed. In the vicinity of the reactants both the adconv-QM/MM and adbf-QM/MM integrated RDFs are close to the fully QM one. At larger distances (starting from 4 Å) the adconv-QM/MM RDF starts to diverge while adbf-QM/MM remains closer to the fully QM result, although the adconv-QM/MM method’s structural error does not significantly affect its free energy profile.

## DISCUSSION AND CONCLUSIONS

The QM/MM approach has been widely used for simulating processes that require a quantum-mechanical description in a small region, for example a reaction with covalent bond rearrangement, within a larger system with important long-range structure, such as a protein or a polar solvent. However, conventional approaches are limited to a fixed QM region, and also contain significant errors in atomic forces near the QM-MM interface as compared with fully QM or fully MM simulations. Making the QM region larger can help by moving the QM-MM interface further away from the region of interest, but may require the methods to become adaptive by allowing molecules to diffuse into or out of the QM region. Such adaptive methods have been developed, but it has proven difficult to make them stable, at least partially because the force errors near the QM-MM interface can unphysically drive particles from one region to the other. To address these issues and enable stable adaptive simulations we have developed the adbf-QM/MM method, which reduces interface errors by



combining forces from two QM/MM calculations with different QM sizes using force-mixing. Here we have described its implementation in the CP2K and AMBER programs, building on their existing QM/MM capabilities. Using the new functionality requires the specification of a few parameters to control the sizes of the core QM, dynamical QM, and buffer regions. The adbf-QM/MM method and its implementations are formulated in a general way, so they can be used with a wide range of QM and MM models as well as different QM/MM coupling methods.

We have tested our implementations using a variety of QM models, including both semi-empirical and density functional theory, on several structural and free energy problems, using conventional QM/MM, adbf-QM/MM, as well as other adaptive methods that forgo the use of some of the QM and/or MM buffer regions. Using the CP2K and AMBER implementations we simulated the structure of bulk water, where we have shown that adbf-QM/MM produces a stable structure in good agreement with fully QM simulations for DFT and for some, but not all, SE methods we tested. A comparison of the free energy profiles of two reactions, water autoprotolysis in the presence of a  $\text{Zn}^{2+}$  ion (SE using AMBER) and dimethyl-phosphate hydrolysis (DFT using CP2K), to fully QM results shows a substantial dependence on the choice of adaptivity, buffers, and details of the QM-MM interaction term. In all cases, the use of a simulation that includes at least one hydration shell beyond the reacting species is important for reproducing the fully QM free energy profile. The water autoprotolysis simulations show some differences between AMBER and CP2K due to their differing QM-MM interactions, but the adbf-QM/MM method gives good agreement with fully QM simulations for both software packages despite these differences. The dimethyl phosphate hydrolysis simulations show that the free energy profiles of the adconv-QM/MM and adbf-QM/MM adaptive method are in good agreement with fully QM results, while the conv-QM/MM and adubf-QM/MM methods are not. The reason for this difference is that the former two methods result in a reasonable solvent structure around the reaction, while the latter two give very different structures. The conv-QM/MM simulation also predicts a qualitatively incorrect metastable state at the transition state collective coordinate value.

In summary, our results show that of the adaptive methods we have tested, the adbf-QM/MM method is the most robust in maintaining reasonable solvent structure and giving

accurate free energy profiles. Adaptive methods that do not include both dynamical QM and buffer regions can also give good structural and free energy profile results for some systems, but they fail to agree with full QM results for other systems. To maximize the accuracy of the adbf-QM/MM method the size of core region should be minimized, the dynamical QM region should include at least one hydration shell around the reaction centre so as to include the most important solvent effects, and the buffer region should be large enough to give forces throughout the dynamical QM region converged to better than a few kcal mol<sup>-1</sup> Å<sup>-1</sup>. Our AMBER and CP2K implementations use a small number of simple parameters to specify the various adaptive regions, and the suggested size criteria can be satisfied with reasonable computational cost, making the adbf-QM/MM method accessible to a wide community of users.

## ACKNOWLEDGMENTS

N.B. acknowledges funding for this work by the Office of Naval Research through the Naval Research Laboratory’s basic research program, and computer time at the AFRL DoD Supercomputing Resource Center through the DoD High Performance Computing Modernization Program (subproject NRLDC04253428). B.L. was supported by EPSRC (grant no. EP/G036136/1) and the Scottish Funding Council. G.C. and B.L. acknowledge support from EPSRC under grant no. EP/J01298X/1. R.C.W. and A.W.G. acknowledge financial support by the National Institutes of Health (R01 GM100934), A.W.G. acknowledges financial support by the Department of Energy (DE-AC36-99GO-10337). This work was partially supported by National Science Foundation (grant no. OCI-1148358) and used the Extreme Science and Engineering Discovery Environment (XSEDE), which is supported by National Science Foundation grant no. ACI-1053575. Computer time was provided by the San Diego Supercomputer Center through XSEDE award TG-CHE130010.

## References

1. A. Warshel and M. Levitt, J. Mol. Biol. **103**, 227 (1976).
2. J. Villá and A. Warshel, The Journal of Physical Chemistry B **105**, 7887 (2001), <http://pubs.acs.org/doi/pdf/10.1021/jp011048h>, URL <http://pubs.acs.org/doi/abs/10.1021/jp011048h>.
3. H. M. Senn and W. Thiel, Angewandte Chemie International Edition **48**, 1198 (2009), ISSN 1521-3773, URL <http://dx.doi.org/10.1002/anie.200802019>.
4. D. Bakowies and W. Thiel, The Journal of Physical Chemistry **100**, 10580 (1996), <http://pubs.acs.org/doi/pdf/10.1021/jp9536514>, URL <http://pubs.acs.org/doi/abs/10.1021/jp9536514>.
5. U. C. Singh and P. A. Kollman, Journal of Computational Chemistry **7**, 718 (1986), ISSN 1096-987X, URL <http://dx.doi.org/10.1002/jcc.540070604>.
6. J. Gao, P. Amara, C. Alhambra, and M. J. Field, The Journal of Physical Chemistry A **102**, 4714 (1998), <http://pubs.acs.org/doi/pdf/10.1021/jp9809890>, URL <http://pubs.acs.org/doi/abs/10.1021/jp9809890>.
7. Y. Zhang, T.-S. Lee, and W. Yang, The Journal of Chemical Physics **110**, 46 (1999), URL <http://scitation.aip.org/content/aip/journal/jcp/110/1/10.1063/1.478083>.
8. O. Akin-Ojo, Y. Song, and F. Wang, Journal of Chemical Physics **129**, 064108 (2008).
9. I. Solt, P. Kulháněk, I. Simon, S. Winfield, M. C. Payne, G. Csányi, and M. Fuxreiter, J. Phys. Chem. B **113**, 5728 (2009).
10. L. Hu, S. Pär, and U. Ryde, J. Chem. Theory Comput. **7**, 761 (2011), URL <http://pubs.acs.org/doi/full/10.1021/ct100530r>.
11. O. Akin-Ojo and F. Wang, J Comput Chem **32**, 453 (2011).
12. T. Kerdcharoen, K. R. Liedl, and B. M. Rode, Chem. Phys. **211**, 313 (1996).

13. T. Kerdcharoen and K. Morokuma, Chem. Phys. Lett. **355**, 257 (2002).
14. B. M. Rode, T. S. Hofer, B. R. Randolph, C. F. Schwenk, D. Xenides, and V. Vchirawongkwin, Theor. Chem. Acc. **115**, 77 (2005).
15. A. Heyden, H. Lin, and D. G. Truhlar, J. Phys. Chem. B **111**, 2231 (2007).
16. A. Heyden and D. G. Truhlar, J. Chem. Theory Comput. **4**, 217 (2008).
17. R. Bulo, B. Ensing, J. Sikkema, and L. Visscher, J. Chem. Theory Comput. **5**, 2212 (2009).
18. S. Yockel and G. C. Schatz, Top. Curr. Chem. **307**, 43 (2011).
19. R. E. Bulo, C. Michel, P. Fleurat-Lessard, and P. Sautet, J. Chem. Theory Comput. **9**, 5567 (2013).
20. N. Bernstein, C. Várnai, I. Solt, S. A. Winfield, M. C. Payne, I. Simon, M. Fuxreiter, and G. Csányi, Phys. Chem. Chem. Phys. **14**, 646 (2012), URL <http://dx.doi.org/10.1039/C1CP22600B>.
21. C. Várnai, N. Bernstein, L. Mones, and G. Csányi, The Journal of Physical Chemistry B **117**, 12202 (2013), <http://pubs.acs.org/doi/pdf/10.1021/jp405974b>, URL <http://pubs.acs.org/doi/abs/10.1021/jp405974b>.
22. B. Ensing, S. O. Nielsen, P. B. Moore, M. L. Klein, and M. Parrinello, Journal of Chemical Theory and Computation **3**, 1100 (2007), <http://pubs.acs.org/doi/pdf/10.1021/ct600323n>, URL <http://pubs.acs.org/doi/abs/10.1021/ct600323n>.
23. G. Csányi, T. Albaret, M. C. Payne, and A. De Vita, Phys. Rev. Lett. **93**, 175503 (2004), URL <http://link.aps.org/doi/10.1103/PhysRevLett.93.175503>.
24. M. Praprotnik, L. Delle Site, and K. Kremer, The Journal of Chemical Physics **123**, 224106 (2005), URL <http://scitation.aip.org/content/aip/journal/jcp/123/22/10.1063/1.2132286>.

25. M. Praprotnik, L. Delle Site, and K. Kremer, Phys. Rev. E **73**, 066701 (2006), URL <http://link.aps.org/doi/10.1103/PhysRevE.73.066701>.
26. A. Jones and B. Leimkuhler, J. Chem. Phys. **135**, 084125 (2011).
27. K. Park, A. W. Gtz, R. C. Walker, and F. Paesani, Journal of Chemical Theory and Computation **8**, 2868 (2012), <http://pubs.acs.org/doi/pdf/10.1021/ct300331f>, URL <http://pubs.acs.org/doi/abs/10.1021/ct300331f>.
28. N. Bernstein, J. R. Kermode, and C. Csányi, Rep Prog Phys **72**, 026501 (2009).
29. <http://cp2k.org/>.
30. D. A. Case, V. Babin, J. T. Berryman, R. M. Betz, Q. Cai, D. S. Cerutti, T. E. Cheatham, III, T. A. Darden, R. E. Duke, H. Gohlke, et al., Tech. Rep., University of California, San Francisco (2014).
31. R. Salomon-Ferrer, D. A. Case, and R. C. Walker, Wiley Interdisciplinary Reviews: Computational Molecular Science **3**, 198 (2013), ISSN 1759-0884, URL <http://dx.doi.org/10.1002/wcms.1121>.
32. A. A. Samoletov, C. P. Dettmann, and M. A. J. Chaplain, Journal of Statistical Physics **128**, 1321 (2007).
33. B. Leimkuhler, E. Noorizadeh, and F. Theil, J Stat Phys **135**, 261 (2009).
34. M. E. Tuckerman, B. J. Berne, G. J. Martyna, and M. L. Klein, The Journal of Chemical Physics **99**, 2796 (1993), URL <http://scitation.aip.org/content/aip/journal/jcp/99/4/10.1063/1.465188>.
35. J. Kastner and W. Thiel, The Journal of Chemical Physics **123**, 144104 (pages 5) (2005), URL <http://link.aip.org/link/?JCP/123/144104/1>.
36. P. Kulhánek, M. Fuxreiter, J. Koča, L. Mones, Z. Střelcová, and M. Petřek, <https://lcc.ncbr.muni.cz/whitezone/development/pmflib/root>.

37. A. D. MacKerell, D. Bashford, M. Bellott, R. L. Dunbrack, J. D. Evanseck, M. J. Field, S. Fischer, J. Gao, H. Guo, S. Ha, et al., *The Journal of Physical Chemistry B* **102**, 3586 (1998), <http://pubs.acs.org/doi/pdf/10.1021/jp973084f>, URL <http://pubs.acs.org/doi/abs/10.1021/jp973084f>.
38. M. J. S. Dewar and W. Thiel, *Journal of the American Chemical Society* **99**, 4899 (1977), <http://pubs.acs.org/doi/pdf/10.1021/ja00457a004>, URL <http://pubs.acs.org/doi/abs/10.1021/ja00457a004>.
39. M. J. S. Dewar, E. G. Zoebisch, E. F. Healy, and J. J. P. Stewart, *Journal of the American Chemical Society* **107**, 3902 (1985), <http://pubs.acs.org/doi/pdf/10.1021/ja00299a024>, URL <http://pubs.acs.org/doi/abs/10.1021/ja00299a024>.
40. K. Nam, Q. Cui, J. Gao, and D. M. York, *Journal of Chemical Theory and Computation* **3**, 486 (2007), <http://pubs.acs.org/doi/pdf/10.1021/ct6002466>, URL <http://pubs.acs.org/doi/abs/10.1021/ct6002466>.
41. M. Korth, *Journal of Chemical Theory and Computation* **6**, 3808 (2010), <http://pubs.acs.org/doi/pdf/10.1021/ct100408b>, URL <http://pubs.acs.org/doi/abs/10.1021/ct100408b>.
42. J. J. P. Stewart, *Journal of Computational Chemistry* **10**, 209 (1989), ISSN 1096-987X, URL <http://dx.doi.org/10.1002/jcc.540100208>.
43. M. Bernal-Uruchurtu and M. Ruiz-Lpez, *Chemical Physics Letters* **330**, 118 (2000), ISSN 0009-2614, URL <http://www.sciencedirect.com/science/article/pii/S0009261400010629>.
44. J. J. P. Stewart, *Journal of Molecular Modeling* **13**, 1173 (2007), ISSN 1610-2940, URL <http://dx.doi.org/10.1007/s00894-007-0233-4>.
45. G. B. Rocha, R. O. Freire, A. M. Simas, and J. J. P. Stewart, *Journal of Computational Chemistry* **27**, 1101 (2006), ISSN 1096-987X, URL <http://dx.doi.org/10.1002/jcc.20425>.

46. D. Porezag, T. Frauenheim, T. Köhler, G. Seifert, and R. Kaschner, Phys. Rev. B **51**, 12947 (1995), URL <http://link.aps.org/doi/10.1103/PhysRevB.51.12947>.
47. T. Laino, F. Mohamed, A. Laio, and M. Parrinello, Journal of Chemical Theory and Computation **1**, 1176 (2005), <http://pubs.acs.org/doi/pdf/10.1021/ct050123f>, URL <http://pubs.acs.org/doi/abs/10.1021/ct050123f>.
48. T. Laino, F. Mohamed, A. Laio, and M. Parrinello, Journal of Chemical Theory and Computation **2**, 1370 (2006), <http://dx.doi.org/10.1021/ct6001169>, URL <http://dx.doi.org/10.1021/ct6001169>.
49. A. D. Becke, Phys. Rev. A **38**, 3098 (1988).
50. C. Lee, W. Yang, and R. G. Parr, Phys. Rev. B **37**, 785 (1988).
51. B. Miehlich, A. Savin, H. Stoll, and H. Preuss, Chem. Phys. Lett. **157**, 200 (1989).
52. S. Grimme, J Comput Chem **27**, 1787 (2006).
53. J. Wang, G. Roman-Perez, J. M. Soler, E. Artacho, and M. V. Fernández-Serra, J Chem Phys **134**, 024516 (2011).
54. S. Goedecker, M. Teter, and J. Hutter, Phys. Rev. B **54**, 1703 (1996), URL <http://link.aps.org/doi/10.1103/PhysRevB.54.1703>.
55. W. Jencks, *Catalysis in Chemistry and Enzymology*, Dover books on physics and chemistry (Dover, 1987), ISBN 9780486654607, URL <http://books.google.co.uk/books?id=LLkSzP-ct0wC>.
56. M. Sprik, Faraday Discuss. **110**, 437 (1998), URL <http://dx.doi.org/10.1039/A801517A>.
57. L. Mones and G. Csányi, The Journal of Physical Chemistry B **116**, 14876 (2012), <http://pubs.acs.org/doi/pdf/10.1021/jp307648s>, URL <http://pubs.acs.org/doi/abs/10.1021/jp307648s>.

58. S. C. Hoops, K. W. Anderson, and K. M. Merz, *Journal of the American Chemical Society* **113**, 8262 (1991), <http://pubs.acs.org/doi/pdf/10.1021/ja00022a010>, URL <http://pubs.acs.org/doi/abs/10.1021/ja00022a010>.
59. W. Thiel and A. Voityuk, *Theoretica chimica acta* **81**, 391 (1992), ISSN 0040-5744, URL <http://dx.doi.org/10.1007/BF01134863>.
60. S. C. L. Kamerlin, P. K. Sharma, R. B. Prasad, and A. Warshel, *Quarterly Reviews of Biophysics* **46**, 1 (2013), ISSN 1469-8994.
61. C. I. Bayly, P. Cieplak, W. Cornell, and P. A. Kollman, *J. Phys. Chem.* **97**, 10269 (1993), <http://pubs.acs.org/doi/pdf/10.1021/j100142a004>, URL <http://pubs.acs.org/doi/abs/10.1021/j100142a004>.
62. W. D. Cornell, P. Cieplak, C. I. Bayly, and P. A. Kollmann, *J. Am. Chem. Soc.* **115**, 9620 (1993), <http://pubs.acs.org/doi/pdf/10.1021/ja00074a030>, URL <http://pubs.acs.org/doi/abs/10.1021/ja00074a030>.
63. V. Hornak, R. Abel, A. Okur, B. Strockbine, A. Roitberg, and C. Simmerling, *Prot. Struct. Funct. Bioinf.* **65**, 712 (2006), ISSN 1097-0134, URL <http://dx.doi.org/10.1002/prot.21123>.
64. P. P. Ewald, *Annalen der Physik* **369**, 253 (1921), ISSN 1521-3889, URL <http://dx.doi.org/10.1002/andp.19213690304>.
65. T. Darden, D. York, and L. Pedersen, *The Journal of Chemical Physics* **98**, 10089 (1993), URL <http://link.aip.org/link/?JCP/98/10089/1>.
66. T. Laino and J. Hutter, *The Journal of Chemical Physics* **129**, 074102 (2008), URL <http://scitation.aip.org/content/aip/journal/jcp/129/7/10.1063/1.2970887>.
67. K. Nam, J. Gao, and D. M. York, *Journal of Chemical Theory and Computation* **1**, 2 (2005), <http://pubs.acs.org/doi/pdf/10.1021/ct049941i>, URL <http://pubs.acs.org/doi/abs/10.1021/ct049941i>.



68. G. d. M. Seabra, R. C. Walker, M. Elstner, D. A. Case, and A. E. Roitberg, *The Journal of Physical Chemistry A* **111**, 5655 (2007), pMID: 17521173, <http://pubs.acs.org/doi/pdf/10.1021/jp0700711>, URL <http://pubs.acs.org/doi/abs/10.1021/jp0700711>.
69. R. C. Walker, M. F. Crowley, and D. A. Case, *Journal of Computational Chemistry* **29**, 1019 (2008), ISSN 1096-987X, URL <http://dx.doi.org/10.1002/jcc.20857>.
70. A. W. Gtz, M. A. Clark, and R. C. Walker, *Journal of Computational Chemistry* **35**, 95 (2014), ISSN 1096-987X, URL <http://dx.doi.org/10.1002/jcc.23444>.
71. S. A. Adelman and J. D. Doll, *J. Chem. Phys.* **64**, 2375 (1976), URL <http://link.aip.org/link/?JCP/64/2375/1>.
72. G. Bussi, D. Donadio, and M. Parrinello, *J. Chem. Phys.* **126**, 014101(1 (2007).
73. S. A. Winfield, Ph.D. Thesis pp. 1–202 (2009).
74. G. Murdachaew, C. J. Mundy, G. K. Schenter, T. Laino, and J. Hutter, *The Journal of Physical Chemistry A* **115**, 6046 (2011), <http://pubs.acs.org/doi/pdf/10.1021/jp110481m>, URL <http://pubs.acs.org/doi/abs/10.1021/jp110481m>.
75. S. Caratzoulas, T. Courtney, and D. G. Vlachos, *The Journal of Physical Chemistry A* **115**, 8816 (2011), <http://pubs.acs.org/doi/pdf/10.1021/jp203436e>, URL <http://pubs.acs.org/doi/abs/10.1021/jp203436e>.
76. C. N. Rowley and B. Roux, *Journal of Chemical Theory and Computation* **8**, 3526 (2012), <http://pubs.acs.org/doi/pdf/10.1021/ct300091w>, URL <http://pubs.acs.org/doi/abs/10.1021/ct300091w>.

# List of Figures

1	Flowchart of the adaptive buffered force QM/MM method. For each configuration during the dynamics two calculations are performed: an extended QM/MM calculation to get accurate forces in the dynamical QM region and a reduced QM/MM calculation (that can be fully MM if corresponding parameters are available) to get converged forces in the dynamical MM region.	36
2	Visualization of the QM regions of an adaptive buffered-force QM/MM simulation of dimethyl-phosphate hydrolysis. The core region is the dimethyl-phosphate and the attacking hydroxide ion (blue) with no additional adaptively selected atoms. The dynamical QM region (red) is selected by extending the core region by $r_{\text{qm}} = 3.0 - 3.5$ Å. The buffer region (green) is an additional layer around the dynamical QM region within $r_{\text{buffer}} = 3.0 - 3.5$ Å. The rest of the system (orange) is treated as MM in both the extended and reduced calculations. Ball-and-stick representation is used for atoms which follow QM forces in the dynamics.	37
3	Basic CP2K (a) and AMBER (b) input files extended by the adbf-QM/MM related keywords of the phosphate system.	38
4	Reaction scheme of the autoprotolysis between a zinc-coordinated and a non-coordinated water molecules (orange).	39
5	Reaction scheme of the dimethyl-phosphate hydrolysis.	39
6	Force convergence on the central oxygen atom in pure bulk water for different SE methods relative to reference forces from calculations using the same SE method with buffer size of 10.0 Å. Top panel shows the mean force error based on 10 independent configurations, and bottom panel shows the maximum error.	39
7	Oxygen–oxygen RDFs in bulk water using different SE methods. Vertical dashed lines at 4.5 Å denote the size of dynamical QM region. For MNDO, a second vertical line at 6.5 Å represents the outer boundary of the dynamical QM region for the larger simulation.	40

8	RDFs and integrated RDFs of bulk water using DFT with different adaptive QM/MM methods. . . . .	41
9	Mean force errors of key atoms in the dynamical QM region ( $r_{\text{qm}} = 3.0 \text{ \AA}$ ) of the water autoprotolysis reaction using the MNDOD model and different sizes of buffer region at the three conv-QM/MM predicted extremum points, relative to forces from a calculation with buffer size of $7.0 \text{ \AA}$ . Force errors on zinc ion (red), donor (green) and acceptor (blue) oxygen atoms and the average of non-reactive oxygen atoms (purple) in the dynamical QM region are shown. . . . .	42
10	Potential of mean force profiles of the water autoprotolysis reaction using MNDOD and the different QM/MM methods as functions of the difference of rational coordination number <i>DRCN</i> . 95% confidence intervals are comparable in size to symbols. Top panel shows results from CP2K including periodic fully SE simulation, and bottom panel shows results from AMBER. . . . .	43
11	Mean force errors of key atoms of the phosphate hydrolysis reaction using DFT and different sizes of buffer region around the phosphate – hydroxide ion system (i.e. $r_{\text{qm}} = 0.0 \text{ \AA}$ ) at three different <i>DD</i> values, relative to reference forces from a calculation with buffer size of $7.0 \text{ \AA}$ . Force errors on phosphorus atom (red), attacking (green) and leaving (blue) oxygen atoms are shown. . .	44
12	Potential of mean force profiles of the phosphate hydrolysis reaction using DFT and the different adaptive QM/MM methods as functions of the distance difference <i>DD</i> , with 95% confidence intervals. . . . .	44
13	Integrated central phosphorus – water oxygen RDF at the transition state corresponding to the fully QM simulation of the phosphate hydrolysis reactions using different adaptive QM/MM methods, with 95% confidence intervals. .	45

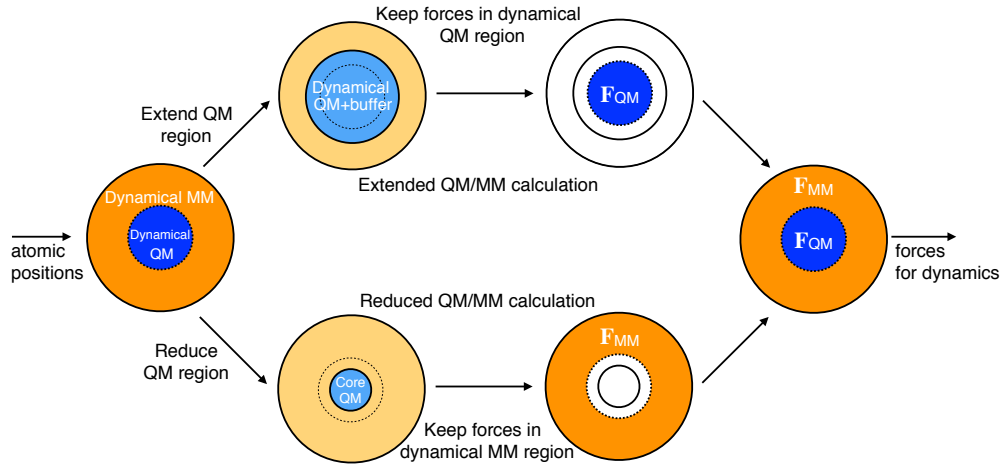


Figure 1: Flowchart of the adaptive buffered force QM/MM method. For each configuration during the dynamics two calculations are performed: an extended QM/MM calculation to get accurate forces in the dynamical QM region and a reduced QM/MM calculation (that can be fully MM if corresponding parameters are available) to get converged forces in the dynamical MM region.

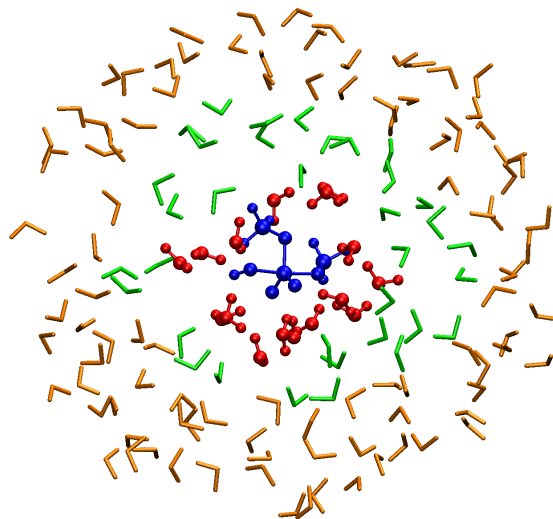


Figure 2: Visualization of the QM regions of an adaptive buffered-force QM/MM simulation of dimethyl-phosphate hydrolysis. The core region is the dimethyl-phosphate and the attacking hydroxide ion (blue) with no additional adaptively selected atoms. The dynamical QM region (red) is selected by extending the core region by  $r_{\text{qm}} = 3.0 - 3.5 \text{ \AA}$ . The buffer region (green) is an additional layer around the dynamical QM region within  $r_{\text{buffer}} = 3.0 - 3.5 \text{ \AA}$ . The rest of the system (orange) is treated as MM in both the extended and reduced calculations. Ball-and-stick representation is used for atoms which follow QM forces in the dynamics.

```

GLOBAL                                ! CP2K: GLOBAL CONTROL SECTION BEGINS
...                                  ! CP2K: KEYWORDS OF GLOBAL CONTROL SECTION
$END GLOBAL                          ! CP2K: END OF GLOBAL CONTROL SECTION
$FORCE_EVAL                          ! CP2K: FORCE_EVAL CONTROL SECTION BEGINS
METHOD QM/MM                         ! CP2K: QM/MM CALCULATION IS ON
...                                  ! CP2K: KEYWORDS OF FORCE_EVAL CONTROL SECTION
$QM/MM                              ! CP2K: QM/MM CONTROL SUBSECTION BEGINS
...                                  ! CP2K: KEYWORDS OF QM/MM CONTROL SUBSECTION
! CP2K-ABFQ/M: DEFINITION OF PERMANENT CORE REGION USING MM INDEXES
$QM_KIND H
  MM_INDEX 2 3 4 11 12 13 15
$END QM_KIND
$QM_KIND C
  MM_INDEX 1 18
$END QM_KIND
$QM_KIND O
  MM_INDEX 5 7 8 9 14
$END QM_KIND
$QM_KIND P
  MM_INDEX 6
$END QM_KIND

! ABFQ/M: ABFQ/M CONTROL SUBSECTION BEGINS
! ABFQ/M: MOMENTUM CONSERVATION TYPE IS EQUAL ACCELERATION
! ABFQ/M: FORCE CORRECTION FOR MM, CONC. IS APPLIED ON ATOMS IN CORE-QM REGION
! ABFQ/M: DEFINITION PERMANENT QM REGION USING MM INDEXES
! ABFQ/M: DEFINITION PERMANENT BUFFER REGION USING MM INDEXES
$FORCE_MIXING
  MOMENTUM_CONSERVATION_TYPE EQUAL_A
  MOMENTUM_CONSERVATION_SECTION ON
  $QM_NON_ADAPTIVE
  $END QM_NON_ADAPTIVE
  $ABUFFER_NON_ADAPTIVE
  R_CORE 8.0 8.0
  R_QM 1.0 1.5
  R_BUF 3.0 3.5
$END FORCE_MIXING
$END QM/MM

! CP2K: MOTION CONTROL SECTION BEGINS
...                                  ! CP2K: KEYWORDS OF MOTION CONTROL SECTION
$MD                                  ! CP2K: MD CONTROL SUBSECTION BEGINS
...                                  ! CP2K: KEYWORDS OF MD CONTROL SUBSECTION
! CP2K: THERMOSTAT CONTROL SUBSECTION BEGINS
$THERMOSTAT
  REGION MASSIVE
  TYPE AD_LANGEVIN
  $AD_LANGEVIN
  TONCON_LANGEVIN 370
  TONCON_MH 74
  $END AD_LANGEVIN
$END THERMOSTAT
! CP2K: END OF THERMOSTAT CONTROL SUBSECTION
$END MD
! CP2K: END OF MOTION CONTROL SECTION

```

(a)

```

&ctrl                                ! sander: main control section begins
...                                  ! sander: keywords of main control section
ntt=2,                                ! abfQM/MM: adaptive massive Langevin thermostat is specified
! ifgt=2,                             ! QM/MM (semieprical) calculation is on
&end                                  ! sander: end of main control section
&qmmm                                ! sander: QM/MM control section begins
...                                  ! sander: keywords of QM/MM control section
! abfQM/MM: abfQM/MM is active
! abfQM/MM: momentum conservation type is equal acceleration
! abfQM/MM: force correction for mm, conc. is applied on atoms in coreqm region
! abfQM/MM: core region inner radius
! abfQM/MM: core region outer radius
! abfQM/MM: qm region inner radius
! abfQM/MM: qm region outer radius
! abfQM/MM: buffer region inner radius
! abfQM/MM: buffer region outer radius
! abfQM/MM: definition of permanent core region using sander mask
! abfQM/MM: definition permanent qm region using sander mask
! abfQM/MM: definition permanent buffer region using sander mask
! abfQM/MM: charge of permanent core region
! abfQM/MM: charge of permanent qm region
! abfQM/MM: charge of permanent buffer region
&end                                  ! sander: end of QM/MM control section

```

(b)

Figure 3: Basic CP2K (a) and AMBER (b) input files extended by the adbf-QM/MM related keywords of the phosphate system.

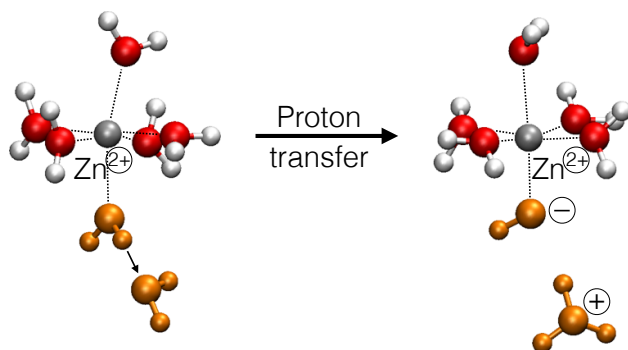


Figure 4: Reaction scheme of the autoprotolysis between a zinc-coordinated and a non-coordinated water molecules (orange).

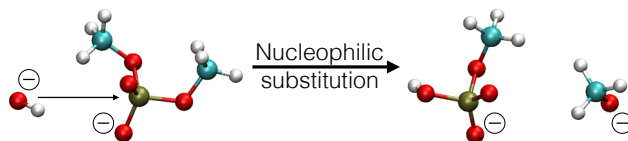


Figure 5: Reaction scheme of the dimethyl-phosphate hydrolysis.

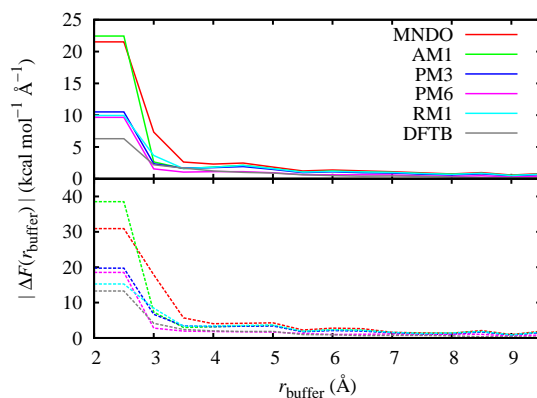


Figure 6: Force convergence on the central oxygen atom in pure bulk water for different SE methods relative to reference forces from calculations using the same SE method with buffer size of 10.0 Å. Top panel shows the mean force error based on 10 independent configurations, and bottom panel shows the maximum error.

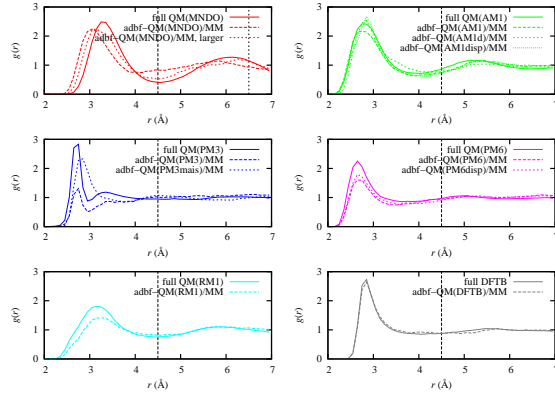


Figure 7: Oxygen–oxygen RDFs in bulk water using different SE methods. Vertical dashed lines at 4.5 Å denote the size of dynamical QM region. For MNDO, a second vertical line at 6.5 Å represents the outer boundary of the dynamical QM region for the larger simulation.



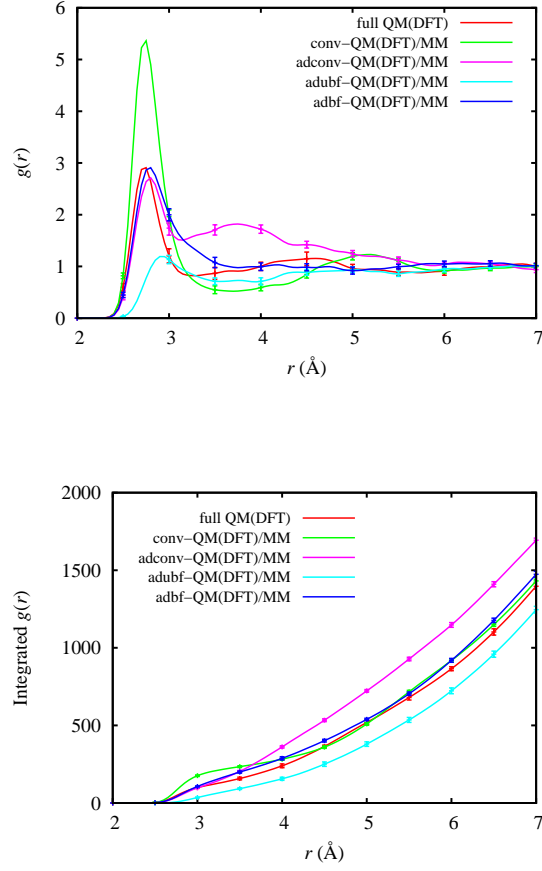


Figure 8: RDFs and integrated RDFs of bulk water using DFT with different adaptive QM/MM methods.

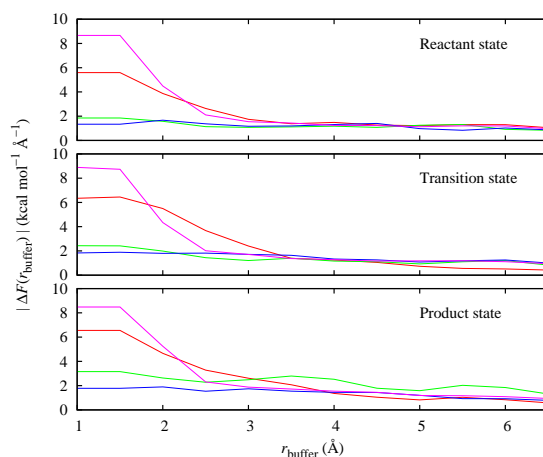


Figure 9: Mean force errors of key atoms in the dynamical QM region ( $r_{\text{qm}} = 3.0 \text{ \AA}$ ) of the water autoprotolysis reaction using the MND0d model and different sizes of buffer region at the three conv-QM/MM predicted extremum points, relative to forces from a calculation with buffer size of  $7.0 \text{ \AA}$ . Force errors on zinc ion (red), donor (green) and acceptor (blue) oxygen atoms and the average of non-reactive oxygen atoms (purple) in the dynamical QM region are shown.

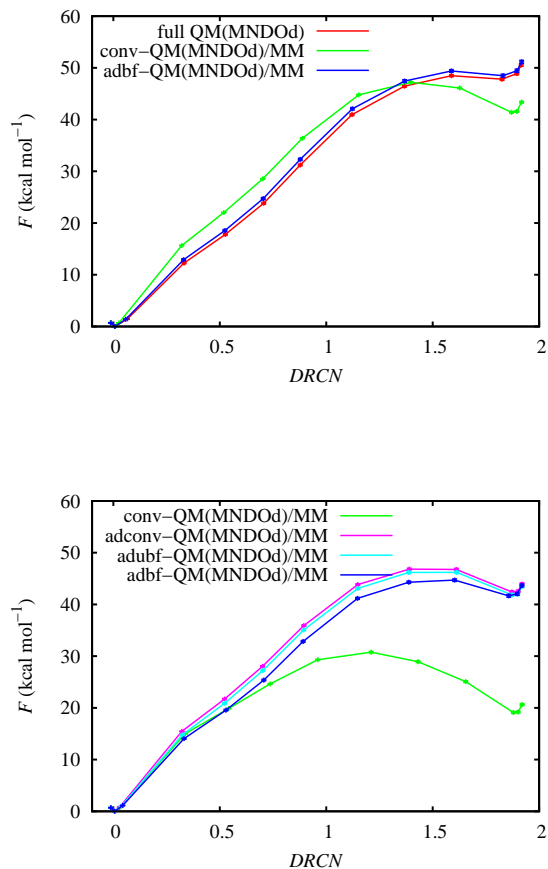


Figure 10: Potential of mean force profiles of the water autoprotolysis reaction using MNDOd and the different QM/MM methods as functions of the difference of rational coordination number  $DRCN$ . 95% confidence intervals are comparable in size to symbols. Top panel shows results from CP2K including periodic fully SE simulation, and bottom panel shows results from AMBER.

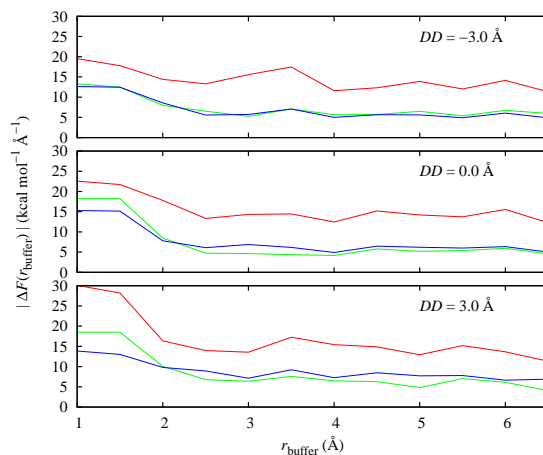


Figure 11: Mean force errors of key atoms of the phosphate hydrolysis reaction using DFT and different sizes of buffer region around the phosphate – hydroxide ion system (i.e.  $r_{\text{qm}} = 0.0$  Å) at three different  $DD$  values, relative to reference forces from a calculation with buffer size of 7.0 Å. Force errors on phosphorus atom (red), attacking (green) and leaving (blue) oxygen atoms are shown.

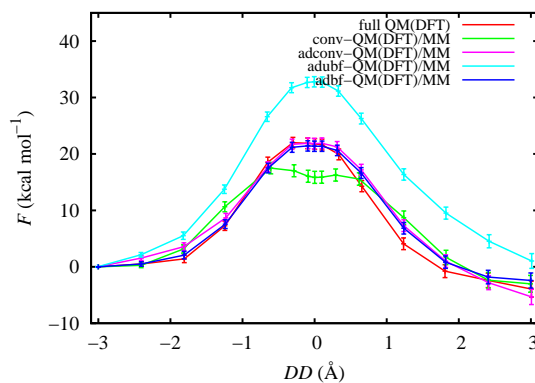


Figure 12: Potential of mean force profiles of the phosphate hydrolysis reaction using DFT and the different adaptive QM/MM methods as functions of the distance difference  $DD$ , with 95% confidence intervals.

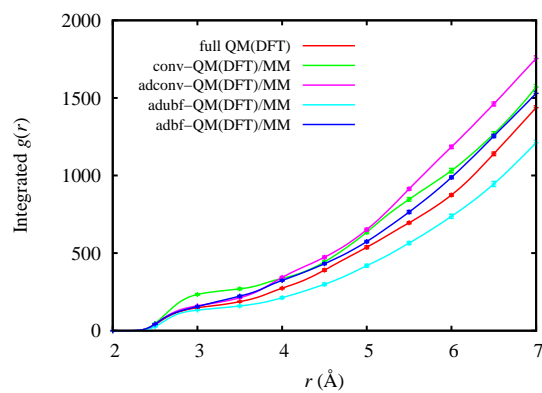


Figure 13: Integrated central phosphorus – water oxygen RDF at the transition state corresponding to the fully QM simulation of the phosphate hydrolysis reactions using different adaptive QM/MM methods, with 95% confidence intervals.